

Supplementary information

1. Supplementary methods: More details on the computation of mantle flow and the plume model

Flow is computed with the method of [1, 2] For the results shown here, we use tomography model *smean* [3], to compute the present-day mantle density field. We use a conversion factor from s-wave speed to density variations $(\delta\rho/\rho)/(\delta v_s/v_s) = 0.2$ below 220 km depth for the fixed-source model and 0.25 for the moving-source model; variations above 220 km depth are not considered. For past times, the density field is somewhat different, as backward-advection of density heterogeneities in the computed flow field is considered for the past 68 Ma. For the time-dependent surface boundary condition, relative plate motions in the South Pacific - Antarctic - Australian region are listed in Table 1. Other rotations are from the compilation of [4, 5], except for Izanagi–Pacific and Kula–Pacific [6], Nazca–Pacific [7] Caribbean–North American, Philippine–Pacific and Phoenix–West Antarctic [8, 9] – see compilations for original references. Absolute motions of the African and Pacific plate are re-determined for times 0-83 Ma through an iteration considering the hotspot motions computed here, optimizing the fit to Tristan and Reunion tracks for African plate motion, and Hawaii and Louisville tracks for Pacific plate motion, using a previously explained method [10]. This iteration converges with sufficient accuracy after one iteration step. We assume intervals of constant rotation rate, and allow for changes of African plate motion at 47 Ma and Pacific plate motion at 25, 47 and 62 Ma. For 83-130 Ma, African absolute plate motions are adopted from [5], before 130 Ma from [11]. Pacific plate motions before 83 Ma are from [12]. Plate motions used to compute hotspot tracks are slightly different from the plate motions used as boundary condition for mantle flow: When computing hotspot tracks, the motion between East and West Antarctic, and between Lord Howe Rise and Pacific is specified (two models), and the fit to all four hotspot tracks is jointly optimized, whereas for the surface boundary condition to mantle flow, we independently determined Pacific and African plate motion, thus introducing additional motion between East and West Antarctica, and between Lord Howe Rise and Pacific. This approach is used because computed tracks are more easily comparable, as hotspot motions are the same in all cases. As a

further difference, lithospheric net rotation is set to zero in the mantle flow boundary condition.

For the spreading ridge system in the Pacific basin, plate boundary locations were computed from the isochrons of [4], using a procedure described in [13]. Plate motions used to rotate isochrons to the past ridge locations are the same as used for mantle flow boundary conditions. In particular, our model does not have a plate boundary between North and South Pacific, as, for example Gordon and Jurdy [8] did. Because some of the isochrons representing plate boundaries close to the Hawaiian hotspot during the Cretaceous have been subducted, this procedure is extended by reconstructing those isochrons, assuming plate geometry and spreading rates stayed the same unless known otherwise. The re-organization of plate boundaries in the North Pacific around 83 Ma ago is modelled following [14], however the Chinook plate is treated as part of the Pacific, rather than a separate plate. Elsewhere, plate boundary locations are from [9]. Computed Hawaiian hotspot motion is noticeably different from the case where plate boundaries from [9] are used everywhere, because around 80 Ma ago, the Hawaiian hotspot was close to a ridge with rather fast spreading rate.

Otherwise, we find that computed hotspot motion is rather insensitive to the plate motion boundary condition. This occurs, because we assume a low asthenospheric viscosity (see below) which somewhat decouples plate motions from mantle flow: whether or not we re-compute plate motions and boundaries taking hotspot motions into account, or whether we independently determine Pacific and African plate motions, or prescribe their relative motion with one of the models introduced here has a rather small effect on the computed flow field and hotspot motion, and does not affect any of our conclusions (Fig. S1).

The mantle is treated as a compressible (moving source model) or incompressible (fixed source model) viscous liquid with phase boundaries, as in [10]. Assuming incompressibility yields higher horizontal flow speeds in the lower mantle, which is, in the fixed source case, necessary to obtain sufficient tilt, hence sufficient southward hotspot motion. Somewhat more vigorous flow at that time beneath the Pacific might have occurred, since flow speeds are not as well constrained as directions of flow and, hence, hotspot motion. Only radial viscosity

variations are considered. We use viscosity “model III” [13], which is consistent with mineral physics and very similar to our initially preferred viscosity structure [15], and yields a mantle flow model that approximately fits geoid, heat flux and postglacial rebound constraints [16]. Very similar mantle flow models can also account for plate motions [17], and explain lithospheric stress [18, 19] and anisotropy in the upper mantle [20]. Given the robustness of these model results and the similarity of the models, we expect that our model would yield very similar results.

The plume base is assumed either to move with the horizontal component of flow, or to be fixed [21, 22]. With the latter assumption, the computed Hawaiian plume conduit is more close to vertical than with a moving source, (except at its base) and thus better matches a recent seismic model [23]; results for computed hotspot motion are very similar or identical in both cases.

We take 11.3°W, 38.7°S for the present location of the Tristan hotspot based on volcanism and radiometric ages on both Tristan da Cunha and Gough Island. We choose 138.1°W, 50.9°S for Louisville, in order to match location and age of the youngest seamount on the Louisville chain. For Hawaii and Reunion, the same present locations as in [10] are used.

Buoyant rising velocity is computed as $u(z) = u_0 \cdot (r/r_0)^2 \cdot \eta_0/\eta(z)$, where $u_0 = 51$ mm/yr, $r_0 = 100$ km, $\eta_0 = 10^{21}$ Pas, $\eta(z)$ is the ambient mantle viscosity, $r = \sqrt[4]{(B/B_0) \cdot (\eta(z)/\eta_0)} \cdot (r_1 + r_{th})$ is plume radius, B is anomalous mass flux, $B_0 = 10^3$ kg/s, $r_1 = 21.6$ km and $r_{th} = 40$ km. Values used for B are the same as in [10]. r increases with depth, as viscosity inside the conduit increases; the conduit is surrounded by a “thermal halo” of thickness r_{th} . This assumption about plume radius is probably more realistic than that of previous models [10]. An even more realistic model [24] based on [25] gives similar results.

Uncertainties of hotspot advection, cannot be formally quantified. Based on our previous studies, we expect that uncertainties in model parameters – in particular mantle viscosity and density structure – cause rather large uncertainties in the speed of mantle flow and hence the magnitude of hotspot motion: It is the amount of hotspot motion that is still compatible with

observed tracks which constrains models, rather than the amount of hotspot motion being constrained by model parameters. On the other hand, the direction of mantle flow, and hence the direction of hotspot motion, is more consistently predicted for various models.

For example, mantle flow is predicted to have caused a southward migration of the Hawaii hotspot through time, and we are able to obtain a good match between predictions and observations of seamounts younger than ~ 47 Ma, and our results are also broadly consistent with paleomagnetic studies for older times [26]. A change of mantle viscosity parameters alters the speed of hotspot migration, but makes little difference to the direction of migration. In contrast, the difference between plate motion chain models 1 to 2 predominantly results in a significant east-west change of the predicted locations of Emperor seamounts.

2. Supplementary discussion: On a possible link between mantle flow and deformation

in Antarctica Here we show results of computations, which are relevant for the question of whether the proposed deformation on the Antarctic plate can be explained by tractions due to mantle flow. Stress computation follows [18] and online supplements. Only tractions due to mantle flow are included here, according to the objective pursued here. In reality, further contributions to the stress field may come from the Gondwana/Antarctic Peninsula subduction zone and the nearby spreading ridge. These are not explicitly accounted for here.

Modeling assumptions are the same as in the main part of the paper for the moving-source hotspot model, except where specifically mentioned. Fig. S2 illustrates forces acting on the lithosphere, and the stresses that are induced within the lithosphere, owing to mantle flow with the present-day density field. The boundary between East and West Antarctica runs from a region of strongly tensile predicted stress (near the Ross Sea), to a region of less tensile stress (near the Antarctic Peninsula), a trend that is consistent with the proposed deformation (extension near Ross Sea, compression near the Antarctic Peninsula). Also, near the Ross Sea, the tractions increase in strength from the West Antarctic to the East Antarctic side of the boundary, whereas it is the other way round near the Antarctic peninsula. Hence the local tractions support the proposed deformation of the boundary.

Fig. S3 shows the same, but based on the density field advected back to 52 Ma. This may seem more appropriate, but the backward advection, neglecting diffusion, viscous heating and other effects, also introduces artifacts. We had previously argued [15] that for the mid-mantle back to about 70 Ma, backward-advection should be a suitable approximation. Since hotspot motion is mostly affected by mid-mantle flow, it is appropriate for that purpose. Lithospheric stresses are however, especially at shorter wavelength, most sensitive to density anomalies in the upper mantle – see e.g. the stress kernels in [18]. Therefore, backward advection is less appropriate for that purpose, since near surface structure is more likely to be influenced by diffusion and local ridge and subduction related small scale flow that is not modelled. However, the boundary between East and West Antarctica still runs from a region of strongly tensile predicted stress near Ross sea, to a region of less tensile stress near the Antarctic peninsula.

Since the hotspots considered in the main part of the paper are all located in the oceans, we had used a viscosity structure that is meant to be appropriate for oceans. If we use instead a somewhat different viscosity structure, with higher viscosities in the asthenosphere, for the stress computations, then, owing to better coupling with mantle flow, somewhat higher magnitudes of tractions and stresses result than in Fig. S2, but the trends discussed above remain the same; they do not depend on the viscosity structure used. We have also computed models without phase boundaries, with an incompressible mantle, and with density fields derived from a number of other tomography models, and found that our results qualitatively stay the same.

References

- [1] Hager, B. H. & O’Connell, R. J. Kinematic models of large-scale flow in the Earth’s mantle. [*J. Geophys. Res.* **84**, 1031-1048 (1979)].
- [2] Hager, B. H. & O’Connell, R. J. A simple global model of plate dynamics and mantle convection. [*J. Geophys. Res.* **86**, 4843-4867 (1981)].

- [3] Becker, T. W. & Boschi, L. A comparison of tomographic and geodynamic mantle models. *Geochem. Geophys. Geosyst.* **3**, 2001GC000168 (2002).
- [4] Royer, J.-Y., Müller, R. D., Gahagan, L. M., Lawver, L. A., Mayes, C. L., Nürnberg, D., and Sclater, J. G., A global isochron chart. *University of Texas Institute for Geophysics Technical Report 117* (1992), online at http://www.es.usyd.edu.au/geology/people/staff/dietmar/Agegrid/digit_isochrons.html
- [5] Müller, R. D., Royer, J.-Y., & Lawver, L. A. Revised plate motions relative to the hotspots from combined Atlantic and Indian Ocean hotspot tracks. *Geology* **21**, 275-278 (1993).
- [6] Gaina, C., Müller, D. & Clark, S. The evolution of global oceanic crust from Jurassic to present day and its contribution to the global carbon budget. paper presented at EGS-EUG-AGU Conference, Nice, France, 2003.
- [7] Tebbens, S. F. & Cande, S. C. Southeast Pacific tectonic evolution from the early Oligocene to Present. *J. Geophys. Res.* **102**, 12,061-12,084 (1997).
- [8] Gordon, R. G. & Jurdy, D. Cenozoic global plate motions. *J. Geophys. Res.* **91**, 12,389-12,406 (1986).
- [9] Lithgow-Bertelloni, C., Richards, M. A., Ricard, Y., O'Connell, R. J. & Engebretson, D. C. Toroidal-poloidal partitioning of plate motions since 120 Ma. *Geophys. Res. Lett.* **20**, 375-378 (1993).
- [10] Steinberger, B. Plumes in a convecting mantle: Models and observations for individual hotspots. *J. Geophys. Res.* **105**, 11127-11,152 (2000).
- [11] Morgan, J. Hotspot tracks and the early rifting of the Atlantic. *Tectonophysics*, **94**, 123-139 (1983).

- [12] Duncan, R. A. & Clague, D. A., Pacific plate motion recorded by linear volcanic chains, in *The Ocean Basins and Margins*, vol. 7a (eds Nairn, A. E. M., Stehli, F. G. & Uyeda, S.) 89-121 (Plenum, New York, 1985).
- [13] Steinberger, B. Motion of the Easter Island hotspot relative to hotspots on the Pacific plate. *Geochem. Geophys. Geosyst.* **3** (11), 8503, doi:10.1029/2002GC000334 (2002).
- [14] Rea, D. K. & Dixon, J. M. Late Cretaceous and Paleogene tectonic evolution of the North Pacific Ocean. *Earth Planet. Sci. Lett.* **65**, 145-166 (1983).
- [15] Steinberger, B. & O'Connell, R. J. Advection of plumes in mantle flow: implications for hotspot motion, mantle viscosity and plume distribution. *Geophys. J. Int.* **132**, 412-434 (1998).
- [16] Steinberger, B. M. & Calderwood, A. R., Mineral physics constraints on viscous flow models of mantle flow. paper presented at European Union of Geosciences XI meeting, Strasbourg, France, 8-12th April 2001.
- [17] Becker, T. W. & O'Connell, R. J., Predicting plate motions with mantle circulation models. *Geochem. Geophys. Geosyst.* **2**, 10.1029/2001GC000171 (2001).
- [18] Steinberger, B., Schmeling, H. & Marquart, G. Large-scale lithospheric stress field induced by global mantle circulation. *Earth Planet. Sci. Lett.* **186**, 75-91 (2001).
- [19] Becker, T. W. & O'Connell, R. J. Lithospheric stresses caused by mantle convection: the role of plate rheology. paper presented at the 2001 Fall Meeting of the American Geophysical Union, 10-14 December, 2001.
- [20] Becker, T. W., Kellogg, J. B., Ekström, G. & O'Connell, R. J. Comparison of azimuthal seismic anisotropy from surface waves and finite-strain from global mantle-circulation models. *Geophys. Journ. Int.*, in press (available at <http://www.seismology.harvard.edu/~becker/>).

- [21] Jellinek, A. M. & Manga, M. The influence of a chemical boundary layer on the fixity, spacing and lifetime of mantle plumes. *Nature* **418**, 760-763 (2002).
- [22] Davaille, A., Girard, F. & Le Bars, M. How to anchor hotspots in a convecting mantle? *Earth Planet. Sci. Lett.* **203**, 621-634 (2002).
- [23] Montelli, R., Nolet, G., Dahlen, F. A., Masters, G., Engdahl, E. R. & Hung, S.-H., Finite-frequency tomography reveals a variety of plumes in the mantle *Science* **303**, 338-343 (2004).
- [24] Antretter, M. Moving hotspots - Evidence from paleomagnetism and modeling. *thesis*, Univ. Munich, München, Germany (2001).
- [25] Albers, M. & Christensen, U. The excess temperature of plumes rising from the core-mantle boundary. *Geophys. Res. Lett.* **23**, 3567-3570 (1996).
- [26] Tarduno J. A. *et al.*, The Emperor Seamounts: A record of southward motion of the Hawaiian hotspot plume in Earth's mantle. *Science* **301**, 1064-1069 (2003).
- [27] Nankivell, A. P. Tectonic evolution of the Southern Ocean between Antarctica, South America and Africa over the past 84 Ma. *PhD thesis*, University of Oxford, Oxford, UK (1997).
- [28] Cande, S. C., Stock, J. M., Mueller, R. D. & Ishihara, T. Cenozoic motion between East and West Antarctica. *Nature* **404**, 145-150 (2000).
- [29] Cande, S. C., Raymond, C. A., Stock, J. & Haxby, W. F. Geophysics of the Pitman Fracture Zone and Pacific-Antarctic plate motions during the Cenozoic. *Science* **270**, 947-953 (1995).
- [30] Larter, R. D., Cunningham, A. P., Barker, P. F., Gohl, K. & Nitsche, F. O. Tectonic evolution of the Pacific margin of Antarctica 1. Late Cretaceous tectonic reconstructions. *J. Geophys. Res.*, **107**, 2345, doi:10.1029/2000JB000052 (2002).

- [31] Tikku, A. A. & Cande, S. C. On the fit of Broken Ridge and Kerguelen Plateau. *Earth Planet. Sci. Lett.* **180**, 117-132 (2000).
- [32] Gaina C. *et al.* The tectonic history of the Tasman Sea; a puzzle with 13 pieces. *J. Geophys. Res.* **103**, 12,413-12,433 (1998).
- [33] Sutherland, R., The Australia-Pacific boundary and Cenozoic plate motions in the SW Pacific; some constraints from Geosat data. *Tectonics* **14**, 819-831 (1995).
- [34] Marks, K. M. & Tikku, A. A. Cretaceous reconstructions of East Antarctica, Africa and Madagascar. *Earth Planet. Sci. Lett.* **186**, 479-495 (2001).
- [35] Livermore R. & Hunter R., Mesozoic seafloor spreading in the Southern Weddell Sea. *Geol. Soc. Spec. Pub.*, **108**, 227-241 (1996).
- [36] Muller, R. D. *et al.* Mesozoic/Cenozoic events around Australia, in *The History and Dynamics of Global Plate Motions*, vol. 121 of *Geophysical Monograph Series*, (eds Richards, M. A., Gordon, R. G. & van der Hilst, R. D.) 161-188 (AGU, Washington D.C., 2000).

Supplementary Table S1. Finite rotation parameters

Plate 1	Plate 2	Age (Ma)	Lat. (°N)	Lon. (°E)	Angle (°)	Ref.	Footnote
EANT	AFR	2.6	5.5	-38.5	0.39	[27]	
EANT	AFR	9.7	6.5	-40.9	1.47	[27]	
EANT	AFR	19.1	9.9	-39.5	3.23	[27]	
EANT	AFR	25.8	9	-38.7	3.88	[27]	
EANT	AFR	33.1	12.4	-40	5.62	[27]	
EANT	AFR	38.4	12.8	-40.8	6.88	[27]	
EANT	AFR	42.5	11.7	-39.6	7.6	[27]	
EANT	AFR	46.3	10.6	-39.8	8.48	[27]	
EANT	AFR	52.4	9	-41.3	9.78	[27]	
EANT	AFR	65.6	-2.9	-41.5	11.88	[27]	
EANT	AFR	71.1	-5.1	-40.2	13.35	[27]	
EANT	AFR	73.6	-3.5	-41	13.82	[27]	
EANT	AFR	79.1	-1.6	-40.9	15.82	[27]	
EANT	AFR	83	-1.8	-38.7	17.92	[27]	
WANT	EANT	26.55	-18.15	-17.85	0	[28]	a
WANT	EANT	33.55	-18.15	-17.85	0.7	[28]	b
WANT	EANT	43.8	-18.15	-17.85	1.7	[28]	b
CAM	WANT	0.78	64.25	-79.06	0.68	[29]	
CAM	WANT	2.58	67.03	-73.72	2.42	[29]	
CAM	WANT	5.89	67.91	-77.93	5.42	[29]	
CAM	WANT	8.86	69.68	-77.06	7.95	[29]	
CAM	WANT	12.29	71.75	-73.77	10.92	[29]	
CAM	WANT	17.47	73.68	-69.85	15.75	[29]	
CAM	WANT	24.06	74.72	-67.28	19.55	[29]	
CAM	WANT	28.28	74.55	-67.38	22.95	[29]	
CAM	WANT	33.54	74.38	-64.74	27.34	[29]	
CAM	WANT	42.54	74.9	-51.31	34.54	[29]	
CAM	WANT	47.91	74.52	-50.19	37.64	[29]	
CAM	WANT	53.35	73.62	-52.5	40.03	[29]	
CAM	WANT	61.1	71.38	-55.57	44.9	[29]	
CAM	WANT	67.67	69.33	-53.44	51.05	[29]	
CAM	WANT	73.62	66.72	-55.04	53.74	[30]	c
CAM	WANT	83	66.72	-55.04	62.0	[30]	

AUS	ANT	46.30	-14.00	-146.66	24.70	[31]
AUS	ANT	53.30	-10.39	-144.41	25.15	[31]
AUS	ANT	60.90	-9.95	-143.48	25.55	[31]
AUS	ANT	71.00	-9.48	-142.98	26.13	[31]
AUS	ANT	79.00	-5.13	-140.20	26.57	[31]
AUS	ANT	83.00	-2.05	-139.21	27.12	[31]
LHR	AUS	50.00	0.00	0.00	0.00	[32]
LHR	AUS	53.30	-14.19	130.41	-0.72	[32]
LHR	AUS	55.80	-15.93	133.47	-2.11	[32]
LHR	AUS	57.90	-16.93	136.23	-3.79	[32]
LHR	AUS	61.20	-4.65	131.51	-4.43	[32]
LHR	AUS	62.50	-4.71	132.68	-5.17	[32]
LHR	AUS	64.00	-0.19	130.37	-5.46	[32]
LHR	AUS	65.60	-3.99	131.80	-6.74	[32]
LHR	AUS	67.70	-9.04	134.46	-8.83	[32]
LHR	AUS	71.10	-14.72	139.04	-13.08	[32]
LHR	AUS	73.60	-9.53	137.20	-12.94	[32]
LHR	AUS	79.10	0.37	133.82	-13.00	[32]
LHR	AUS	83.00	1.57	133.42	-13.04	[32]
LHR	CAM	46.3	-49.8	178.4	-49.0	[33]
LHR	CAM	83.	-49.8	178.4	-49.0	[33]
CAM	PAC	83.0	0.	0.	0.	

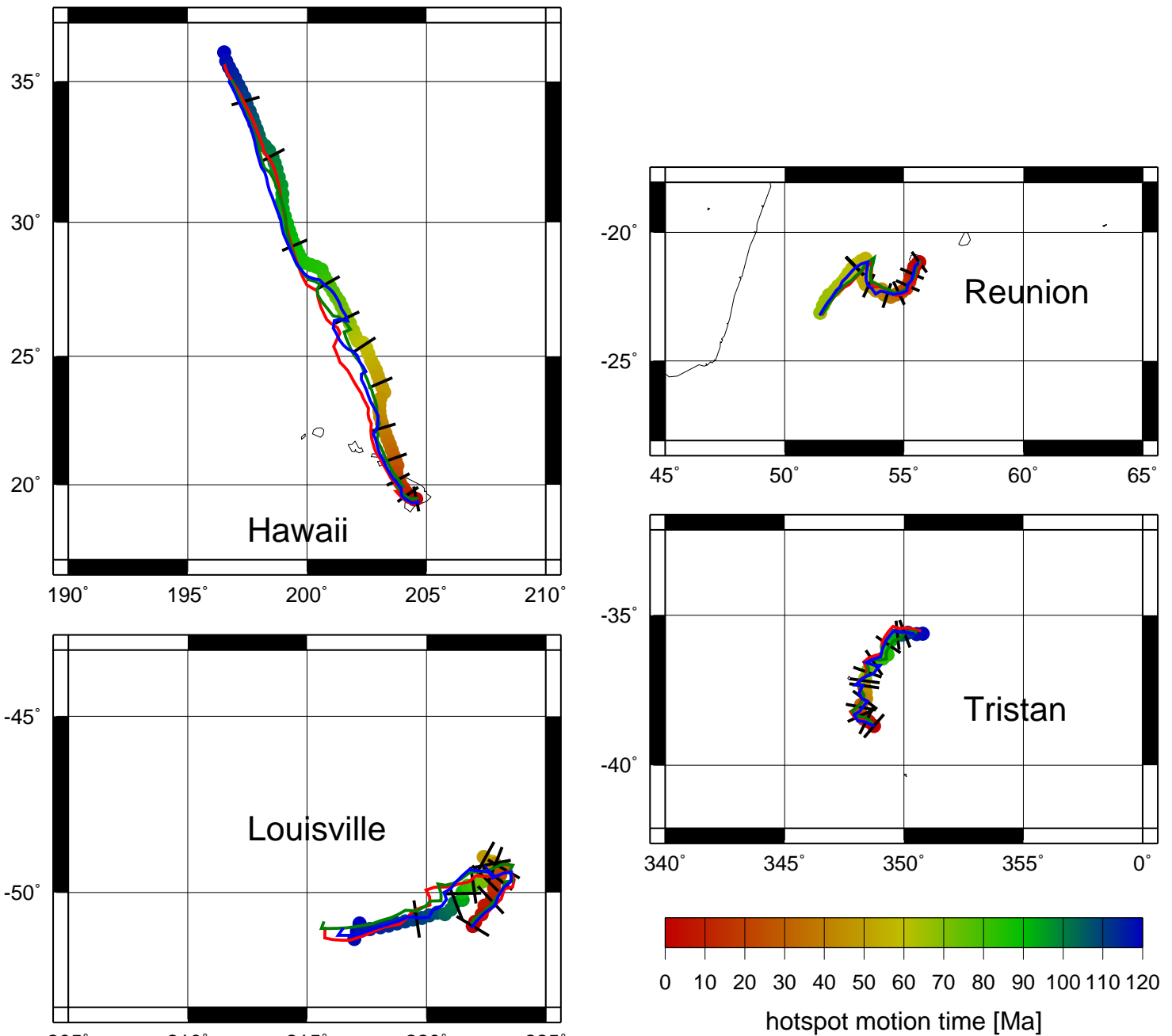
AFR = Africa, EANT = East Antarctica (Dronning Maud Land, Northern Victorialand),
WANT = West Antarctica (Marie Byrd Land), CAM = Southern Campbell Plateau, AUS =
Australia, LHR = Lord Howe Rise, PAC = Pacific.

a: End of Antarctic deformation at chron 8o.

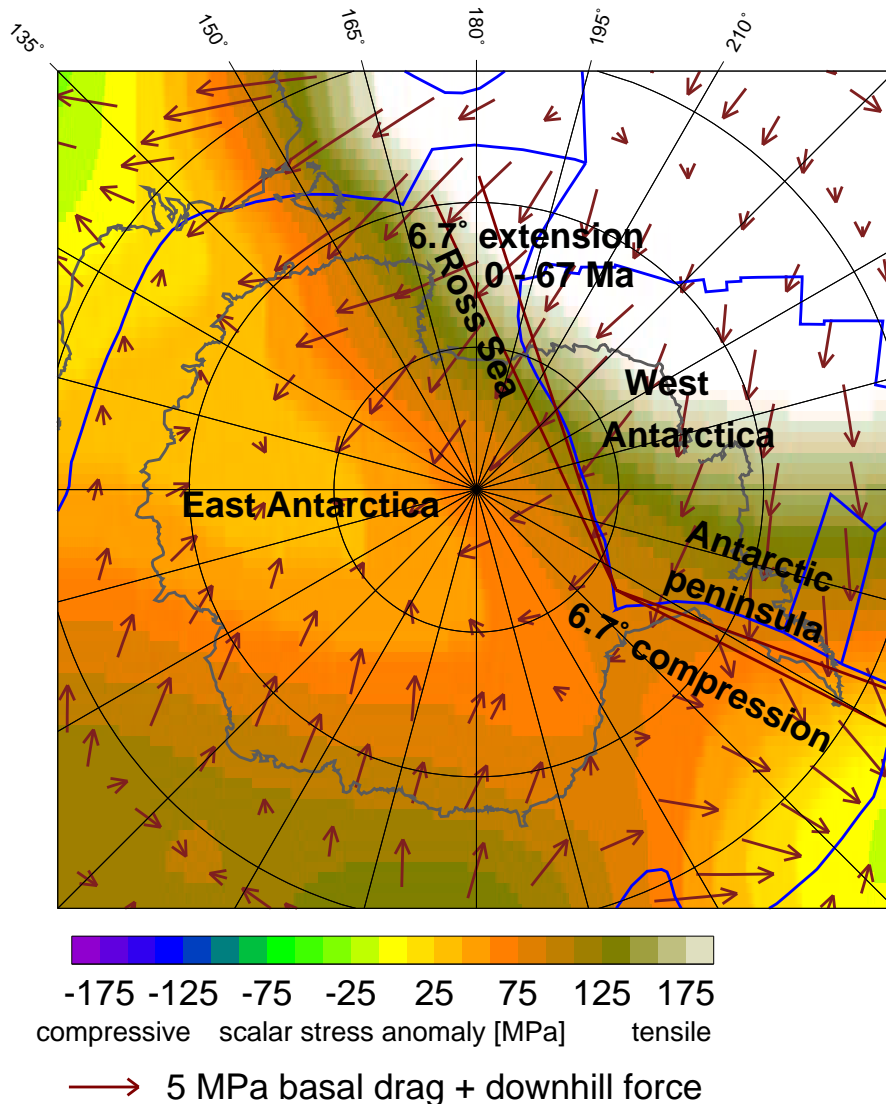
b: Reconstruction of Adare Basin at chron 13o, three-plate solution for WANT-AUS-EANT.

c: reported from Joann Stock, unpublished manuscript

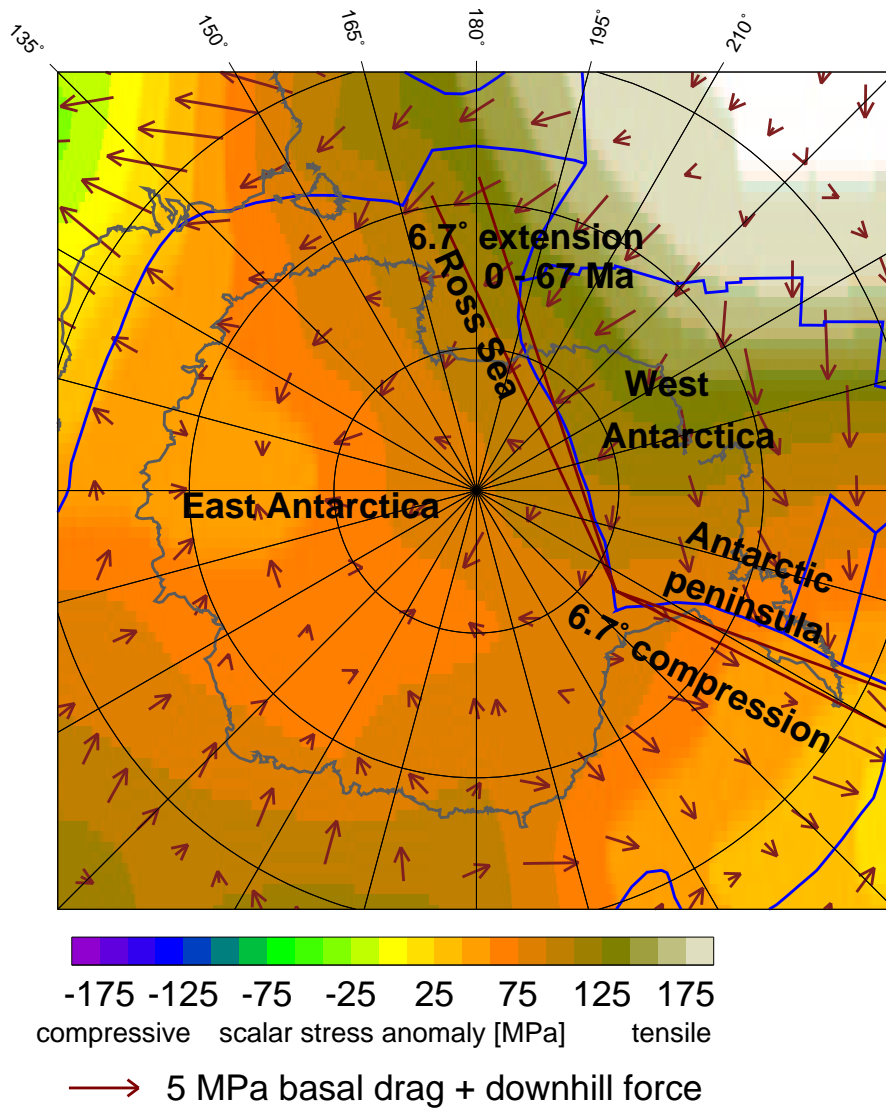
Only those rotations relevant for plate motion chain models 1 and 2 are included. For the plate motion boundary condition for flow for earlier times [4, 34, 35] for EANT - Africa, [36] for AUS-ANT are used.



Supplementary Figure S1 Dependence of hotspot motion on computed plate motion boundary condition. Rainbow-colored lines are the same as in Fig. 2. For the single-colored lines, we use after 83 Ma the plate motion models that were used to construct the hotspot tracks of the same color shown in Fig. 2 instead.



Supplementary Figure S2 Traction and stresses for a 100 km thick lithosphere, due to mantle flow for the present-day density field. Arrows indicate the sum of basal tractions on the lithosphere and downhill forces due to dynamic topography. In order to best illustrate the forces acting on plates, we assume zero plate motions here – if we would assume freely moving plates instead, forces acting on each plate would add up to zero. Colors indicate the predicted stresses within the lithosphere. Also shown (in blue) are plate boundaries at 52 Ma, which were constructed as explained in supplementary section 1. Where isochrons have been subducted, boundaries of the Pacific spreading ridge system are usually connected to the closest point of the circum-Pacific boundary, therefore the Phoenix plate is very small in this reconstruction. Present-day continental outlines are rotated back to 52 Ma, using the plate motion model 2 with fit to all hotspot tracks, as for the blue lines in Fig. 2. They do not exactly correspond to the plate boundary between Antarctica and Australia, since that was reconstructed without consideration of hotspot motion. The proposed deformation is schematically illustrated. Since the pole of relative plate rotation in Table S1 is with respect to the present position of Antarctica, it has been moved accordingly. Place names mentioned in the text are shown.



Supplementary Figure S3 Same as Fig. S2, but for the density field advected back in time to 52 Ma.